THE JOURNAL OF PHYSICAL CHEMISTRY B

Article

pubs.acs.org/JPCB

Theoretical Study of the Preferential Solvation Effect on the Solvatochromic Shifts of *para*-Nitroaniline

Samuel Frutos-Puerto, Manuel A. Aguilar, and Ignacio Fdez. Galván*

Química Física, Edif. José María Viguera Lobo, Universidad de Extremadura, Avda. de Elvas s/n, 06071 Badajoz, Spain

ABSTRACT: The origin of the nonlinear solvatochromic shift of *para*-nitroaniline was investigated using a mean-field sequential QM/MM method, with electron transitions computed at the CASPT2/cc-pVDZ level. Experimental data shows that the solvatochromic shift has a strong nonlinear behavior in certain solvent mixtures. We studied the case of cyclohexane–triethylamine mixtures. The results are in good agreement with the experiments and correctly reproduce the nonlinear variation of the solvent shift. Preferential solvation is clearly observed, where the local solvent composition in the neighborhood of the solute is significantly different from the bulk. It is found that even at low triethylamine concentrations a strong hydrogen bond is formed between *para*-nitroaniline and triethylamine, and cyclohexane is practically absent from the first solvation layer already at a molar fraction of 0.6 in triethylamine. The hydrogen bond formed is sufficiently long-lived to determine an asymmetric environment around the solute molecule. The resulting nonlinear solvent effect is mainly due to this hydrogen bond influence, although there is also a small contribution from dielectric enrichment.

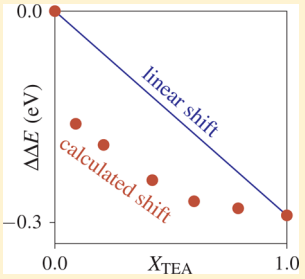

INTRODUCTION

It is well-known that the thermodynamic and spectral properties of molecules can be modified in the presence of a solvent. In particular, the maxima in UV/vis absorption or fluorescence spectra can be shifted to higher or lower frequencies when a molecule is immersed in a solvent, a phenomenon that is known as solvatochromic shift.[1] The study of solvent effects on UV/vis spectra provides an important insight on the electronic properties of molecules, and on the nature of the solute–solvent and solvent–solvent interactions; however, their theoretical study represents an important challenge, since it requires both an accurate description of the internal structure of the solute and an appropriate modeling of the solvent structure and the solute–solvent interactions. As a first approximation, the solvent effect can be considered proportional to its polarity, usually described through the macroscopic dielectric constant and refractive index (or their polarity functions $f(x) = 2(x - 1)/(2x + 1)$, where $x = \varepsilon$ or $x = n^2$). There are, however, many systems where other factors are involved such as specific interactions, which are a consequence of the chemical nature of the solute and solvent molecules, rather than macroscopic quantities. The most important type of specific interaction is hydrogen bonding, but there may be others like π–π stacking, dipole–dipole interactions, σ–hole bonding, etc.[2]

The case of solvent mixtures is particularly interesting, because the overall polarity can be continuously modified by changing the mixture composition. In an ideal mixture, the polarity is additive and changes linearly with the molar fractions, but even in these cases, it can be found that solvatochromic shifts do not vary linearly with the molar fractions or with the bulk polarity. This is generally attributed to "preferential solvation", where the local composition of the mixture in the neighborhood of the solute molecule is different from the bulk composition. Preferential solvation, in turn, can be due to specific interactions. However, even in the absence of such specific interactions, a polar solute can induce a change in the composition of its environment in a process called "dielectric enrichment".[3]

The quantitative description of nonlinear effects in solvent mixtures is generally done by assuming the establishment of different solvent–solvent and solvent–solute equilibria, corresponding to the formation of various possible molecular associations. The observed properties depend on the proportion of the different associations, and the resulting parameters are fitted to experimental data.[4−6] This approach can be useful to explore and understand the interactions that take place in a solvent mixture, but it is lacking in predictive capability. Simulation methods such as molecular dynamics, on the other hand, can reproduce the microscopic structure and features of the solvent mixture, as long as the force field employed is able to model the different kinds of interactions present in the system. Purely classical simulations have been used, for example, to study the nonlinear behavior of the nuclear Overhauser effect (NOE) in solvent mixtures.[7]

When studying solvatochromic shifts, however, it is essential to apply high-level quantum methods for the description of the electronic states involved. The treatment of nonlinear effects in solvent mixtures is not straightforward in quantum calculations, because the most popular solvent models (such as PCM (polarizable continnum model),[8] COSMO (conductor-like screening model),[9] or the SCRF (self-consistent reaction field) method[10]) are based on a structureless continuum, and therefore disregard the microscopic structure of the solvent.[11]

Received: November 6, 2012
Revised: January 23, 2013
Published: January 23, 2013

   dx.doi.org/10.1021/jp310964k | *J. Phys. Chem. B* 2013, 117, 2466–2474

The usual ways to overcome this limitation involve including explicit solvent molecules in the quantum calculation to describe specific interactions, or using a local or nonuniform dielectric constant to take into account dielectric enrichment.[12] However, these solutions require at least a prior qualitative knowledge of the effect that one is trying to investigate in order to set up a correct calculation. More appropriate are methods that do not reduce the solvent to a structureless continuum but keep an atomistic description of the solvent molecules, usually through molecular mechanics models. However, for the study of electronic transitions, high-level quantum methods must be used for the quantum calculations, which often precludes the use of conventional QM/MM methods, as they would demand too high a computational effort. A group of QM/MM methods that apply what is generally known as the mean field approximation have proved to be a very efficient and successful choice for this kind of study, since they allow the number of quantum computations needed to be drastically reduced while retaining most of the details of the solvent structure (see the recent works by Yamamoto et al.[13,14]). In this group, we can also include RISM-SCF[15,16] (reference interaction site model self-consistent field) or OFE/RISM[17,18] (orbital-free embedding RISM), S-QM/MM combined with ASEC[19,20] (sequential QM/MM, averaged solvent electrostatic configuration), and ASEP/MD[21−23] (averaged solvent electrostatic potential from molecular dynamics), the latter of which has been developed in our research group.

In this work, we will study the nonlinear solvatochromic shift of the first absorption band of *para*-nitroaniline (PNA) in a mixture of two solvents of similar low dielectric constant, cyclohexane (CH) and triethylamine (TEA). The structure of PNA contains both an electron-donating and -withdrawing group, connected through an aromatic ring, so that the first absorption band leads to an excited state of intramolecular charge transfer character, with a high dipole moment. The large increase in dipole moment during the transition makes its energy quite sensitive to the solvent polarity and other changes in the solute environment, so it is a good target for solvent effect studies. Although CH and TEA are characterized by similar dielectric constants, they differ in a key aspect: the TEA molecules can act as hydrogen-bond acceptors, allowing the formation of these specific interactions with the PNA molecules, as discussed by other authors.[24,25]

Our goal in this work is to answer the following questions: Is there preferential solvation in this system? Is this preferential solvation related to the formation of hydrogen bonds between PNA and TEA? Which is the role of dielectric enrichment? Is preferential solvation responsible for the nonlinear behavior? By answering these questions, we also expect to prove the ability of ASEP/MD (and similar methods) to describe the nonlinear effects that occur in solvent mixtures, without introducing additional empirical parameters or assumptions.

METHODS AND DETAILS

Solvent effects on the PNA absorption were calculated with the ASEP/MD (average solvent electrostatic potential from molecular dynamics) method. This is a sequential quantum mechanics/molecular mechanics (QM/MM) method implementing the mean field approximation. It combines a high-level quantum mechanics (QM) description of the solute with a classical molecular mechanics (MM) description of the solvent, such that QM and MM calculations are not simultaneous but sequential. Since it makes use of the mean field approximation, the solvent effect is introduced into the solute's wave function as an average perturbation. Details of the method have been described in previous papers,[21−23] so here we will only present a brief outline.

As mentioned above, ASEP/MD is a method combining QM and MM descriptions. During the MD simulations, all molecules are represented with a classical force field, the intramolecular geometry of the solute is considered fixed, and its electron distribution is represented through point charges. From the resulting simulation data, the average electrostatic potential generated by the solvent molecules on the space occupied by the solute (ASEP) is obtained. This potential is introduced as a set of external point charges into the molecular Hamiltonian of the solute molecule. By solving the associated Schrödinger equation, one gets a new charge distribution for the solute. The new charge distribution can be used in another MD simulation, and this iterative process is repeated until the electron distribution of the solute and the solvent structure around it are mutually equilibrated.

The ASEP/MD framework can also be used to optimize the geometry of the solute molecule.[26] At each QM calculation, the gradient and Hessian on the system's free-energy surface (including the van der Waals contribution, from the MM force field) can be obtained, and thus, they can be used to search for stationary points on this surface by some optimization method. In the computation of the gradient and Hessian, the free-energy gradient method[27] is used, with the incorporation of the mean field approximation to reduce the number of quantum calculations needed. In this way, after each MD simulation, the solute geometry is optimized within the fixed "average" solvent structure by using the free-energy derivatives. In the next MD simulation, the new solute geometry and charge distribution are used. This approach allows the optimization of the solute geometry in parallel to the solvent structure.

For calculating vertical transition energies, the Franck−Condon principle is assumed. The iterative process is only performed on the initial state of the transition (the ground state for absorption); i.e., the charge distribution and the energy derivatives of the solute are calculated for the initial state's wave function. Once the equilibrium solvation of the initial state is obtained, the final energies of the different electronic states are calculated with a frozen solvent model; that is, all states are computed within the same set of external point charges representing the solvent and with a static solute geometry.

With the transition energies calculated in solution (ΔE) and in the gas phase (ΔE^0), the solvatochromic shift δ can be obtained as the difference

$$\begin{aligned}\delta &= \Delta E - \Delta E^0 \\ &= (\langle \Psi_{ex}|\hat{H}_{QM} + \hat{V}|\Psi_{ex}\rangle - \langle \Psi_g|\hat{H}_{QM} + \hat{V}|\Psi_g\rangle + \Delta E^{ne}) \\ &\quad - (\langle \Psi^0_{ex}|\hat{H}^0_{QM}|\Psi^0_{ex}\rangle - \langle \Psi^0_g|\hat{H}^0_{QM}|\Psi^0_g\rangle) \\ &= (\langle \Psi_{ex}|\hat{H}_{QM} + \hat{V}|\Psi_{ex}\rangle - \langle \Psi^0_{ex}|\hat{H}^0_{QM}|\Psi^0_{ex}\rangle) \\ &\quad - (\langle \Psi_g|\hat{H}_{QM} + \hat{V}|\Psi_g\rangle - \langle \Psi^0_g|\hat{H}^0_{QM}|\Psi^0_g\rangle) + \Delta E^{ne} \end{aligned} \quad (1)$$

where the subindices ex and g denote the excited and ground state states of the transition, $\hat{H}_{QM}$ is the QM Hamiltonian of the solute at the in-solution geometry, without the solute−solvent interaction, $\hat{V}$, and $\hat{H}^0_{QM}$ is the QM Hamiltonian at the gas-phase geometry; Ψ and Ψ^0 are, respectively, the wave functions optimized in solution and in the gas phase. ΔE^{ne} collects the contribution of the non-electrostatic solute−solvent interaction

dx.doi.org/10.1021/jp310964k | J. Phys. Chem. B 2013, 117, 2466−2474

terms to the transition energy in solution. The total solvent shift can be partitioned in different contributions, namely, a geometry contribution δ_{geo}, an electronic distortion contribution δ_{dist}, an electrostatic solute−solvent contribution δ_{int}, and a non-electrostatic contribution δ_{ne}. If we introduce Ψ' as the wave function optimized for the $\hat{H}_{QM}$ Hamiltonian (the geometry in solution but without solute−solvent interaction):

$$\delta = \delta_{geo} + \delta_{dist} + \delta_{int} + \delta_{ne}$$

$$\delta_{geo} = (\langle \Psi'_{ex}|\hat{H}_{QM}|\Psi'_{ex}\rangle - \langle \Psi^0_{ex}|\hat{H}^0_{QM}|\Psi^0_{ex}\rangle) - (\langle \Psi'_{g}|\hat{H}_{QM}|\Psi'_{g}\rangle - \langle \Psi^0_{g}|\hat{H}^0_{QM}|\Psi^0_{g}\rangle)$$

$$\delta_{dist} = (\langle \Psi_{ex}|\hat{H}_{QM}|\Psi_{ex}\rangle - \langle \Psi'_{ex}|\hat{H}_{QM}|\Psi'_{ex}\rangle) - (\langle \Psi_{g}|\hat{H}_{QM}|\Psi_{g}\rangle - \langle \Psi'_{g}|\hat{H}_{QM}|\Psi'_{g}\rangle)$$

$$\delta_{int} = \langle \Psi_{ex}|\hat{V}|\Psi_{ex}\rangle - \langle \Psi_{g}|\hat{V}|\Psi_{g}\rangle$$

$$\delta_{ne} = \Delta E^{ne} = E^{ne}_{ex} - E^{ne}_{g} \simeq 0 \quad (2)$$

Thus, δ_{geo} is the solvent shift due to the change in geometry between gas phase and solution, δ_{dist} corresponds to the difference in the solvent-induced wave function distortion energy between the excited and ground states, and δ_{int} corresponds to the difference in solute−solvent electrostatic interaction energy. The van der Waals component of the interaction energy is included in δ_{ne}, but we adopt the approximation of considering it constant for all electronic states of the solute, and therefore, it vanishes when vertical transition energies are considered.

Computational Details. The geometry of PNA was optimized in the gas phase and in solution with the MP2 method, using Dunning's cc-pVDZ basis set. All calculations in solution, including geometry optimization, were done with the ASEP/MD method. All transition properties were computed with multiconfigurational methods and the same basis set. First, the complete active space self-consistent field (CASSCF) method[28] was applied, by including all configurations resulting from the distribution of 12 electrons in 10 orbitals. The active space was the complete π system, comprising the perpendicular atomic p valence orbitals of the 10 heavy atoms. The orbitals were optimized with a state-average (SA) of the first five singlet states, with equal weights. It is known that, in order to obtain accurate transition energies, it is necessary to include the dynamic electron correlation in the quantum calculations, which we did with the complete active space second-order perturbation (CASPT2) method,[29,30] using the SA(5)-CASSCF(12,10) wave function as a reference. To facilitate comparison with experimental values, we report here only results obtained without applying the IPEA (ionization potential − electron affinity) shift to the zeroth-order Hamiltonian.[31] As it has been found and discussed in other works,[32−36] the difference between the IPEA-shifted and non-IPEA-shifted results is almost constant, and the conclusions are hardly affected by this choice. To minimize the appearance of intruder states, an additional imaginary shift of $0.1iE_h$ was used. No symmetry was assumed in any case.

The MD simulations were carried out with rigid solvent and solute molecules. Test simulations with flexible solvent molecules showed that both species maintain their selected conformations in a great extent throughout the simulation time. Lennard-Jones parameters and solvent atomic charges were taken from the OPLS-AA (optimized potentials for liquid simulations, all atoms) force field,[37] and solute atomic charges were calculated from the quantum calculations through a least-squares fit to the electrostatic potential obtained at the points where the solvent charges are located. The geometry of the solvent molecules, cyclohexane (in chair conformation) and triethylamine, was optimized in the gas phase, at the MP2/cc-pVDZ level. A cubic simulation box of approximately 35 Å sides was used in all cases, with a single PNA molecule and a variable number of CH and TEA molecules, depending on the desired molar fraction in TEA (X_{TEA}, see Table 1). Simulations were performed with periodic boundary conditions in the *NVT* ensemble, using a constant density calculated by linear interpolation between the experimental densities of the pure solvents, and the temperature was fixed at 298.15 K with a Nosé−Hoover thermostat. Spherical cutoffs were used to truncate interatomic interactions at around 12.6 Å, and long-range interactions were calculated using the Ewald sum technique. A time step of 0.5 fs was used during the simulations, and each one was run for 50 ps after 25 ps of equilibration.

Table 1. Number of Molecules of Each Solvent, Cyclohexane (CH) and Triethylamine (TEA), Used in the Simulations for the Different Compositions Studied, Identified by Their TEA Molar Fraction Values, X_{TEA}

X_{TEA}	CH	TEA
(CH) 0.00	250	0
0.09	215	20
0.21	170	45
0.42	125	90
0.60	85	130
0.79	45	170
(TEA) 1.00	0	195

At each step of the ASEP/MD procedure, 500 configurations evenly distributed from the MD run were used to calculate the ASEP. The charges from each solvent molecule were kept explicitly whenever the molecule's center of mass was closer than 9 a_o to any solute nucleus; the effect of the farther molecules was included in an additional shell of fitted charges. Each ASEP/MD run was continued until the energies and solute geometry and charges were stabilized for at least five iterations (10−15 iterations in total), and results are reported as the average of these last five iterations, corresponding to an effective simulation time of 250 ps (after equilibrium).

For in solution calculations, a development version of the ASEP/MD software[22] was used. All quantum calculations were performed with Molcas 6.4.[38] All MD simulations were performed using Moldy.[39]

RESULTS AND DISCUSSION

The geometry of the PNA ground state was optimized in the gas phase as well as in the different solvents and mixtures studied in this work. The main geometric parameters in the gas phase and in the two pure solvents cyclohexane (CH) and triethylamine (TEA) are listed in Table 2, and the structure and atom numbering of the solute are displayed in Figure 1. For comparison, in Table 2, we also show the experimental values obtained from the crystallographic structure.[40] It can be seen that there are two fundamental differences between the computed geometry in the gas phase and the experimental geometry in the crystal. First, in the crystal, the bonds C_4−N_9,

dx.doi.org/10.1021/jp310964k | J. Phys. Chem. B 2013, 117, 2466−2474

Table 2. Main Geometrical and Dipolar Parameters of PNA in the Ground State in the Gas Phase, in Two Solvents, and in the Crystal Structure[a]

	gas	CH	TEA	crystal (exp.)[40]
C_1-C_2	1.400	1.399	1.401	1.39
C_2-C_3	1.399	1.399	1.398	1.37
C_3-C_4	1.413	1.412	1.416	1.41
C_4-N_9	1.400	1.398	1.386	1.35
N_9-H	1.018	1.018	1.022, 1.019	1.01
C_1-N_{10}	1.475	1.473	1.469	1.45
$N_{10}-O$	1.233	1.233	1.234	1.23
ϕ(H−N_9−C_4−C3)	29.4	29.2	25.9	0
μ	5.70	5.72	6.93	

[a]Bond distances in ångströms, dihedral angle in degrees, and dipole moment in debyes.

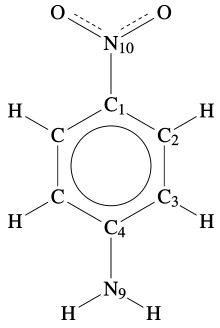

Figure 1. Atom numbering of the *para*-nitroaniline molecule.

C_2-C_3, and C_1-N_{10} are shorter than in gas phase, and second, the NH_2 group is coplanar with the rest of the molecule in the crystal, while in the gas phase it is predicted to be pyramidalized. These differences can be attributed to the intermolecular interactions present in the crystal, where the molecules have a head−tail orientation,[41,42] which favors a quinoidal resonant form, as shown in Figure 2.

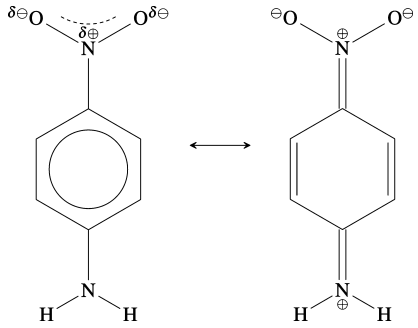

Figure 2. Main resonance structures of *para*-nitroaniline. Left, canonical; right, quinoidal.

In CH solution, the geometry of PNA is predicted practically identical to the gas phase, due to the very weak electrostatic interactions between solute and solvent. On the contrary, when the geometry is optimized in TEA, the geometry resembles more the crystal structure (lengthened C_2-C_3 bond, more planar NH_2). The TEA molecules can act as hydrogen bond acceptors stabilizing the quinoidal resonant structure,[43] which is manifested in an increased dipole moment as well. Similar changes in the optimized geometry are found when the solvent polarity is increased; in this case, a more polar solvent favors structures with charge separation, such as the quinoidal structure of Figure 2, even in the absence of hydrogen bonding.[44,45] A significant feature of our results in TEA solution is the different lengths of the two N−H bonds; the TEA molecules are bulky, and the formation of a second hydrogen bond is difficult. Furthermore, the hydrogen bonds formed with PNA are strong enough that a single solvent molecule remains bonded to one of the hydrogens during most of the simulation, which results in the observed asymmetry of the NH_2 group. This will be further discussed later on.

Next, the five lowest singlet electronic states of PNA were computed in the gas phase at the optimized ground state geometry. Their relative energies and dipole moments are shown in Table 3. The experimental gas-phase absorption

Table 3. Absorption Energies (ΔE, in eV), Oscillator Strengths (f), and Dipole Moments (μ, in D) of PNA in the Gas Phase, Calculated at the CASPT2//MP2 Level

	ΔE	f	μ	ΔE (exp.)[46]
S_0	0.00		5.11	
S_1	4.32	0.003	5.14	
S_2	4.33	0.316	11.47	4.24
S_3	5.81	0.016	2.89	5.66
S_4	6.45	0.045	2.68	

spectrum of PNA is dominated by a band at 4.24 eV.[46] This band is in good agreement with the calculated $S_0 \rightarrow S_2$ transition, both in position and intensity (oscillator strength). The CASPT2//MP2/cc-pVDZ predicted value for the $S_0 \rightarrow S_3$ transition is also in relatively good agreement with the experimental band located at 5.66 eV. These results show that the main features of the PNA spectrum in the gas phase are well reproduced by the present calculations. EOM-CCSD/6-31+G* calculations performed by Kosenkov and Slipchenko[47] gave very similar values. We note that other authors have already shown that the inclusion of diffuse functions does not significantly change the results, since the transitions studied are limited to valence states.[45]

The $S_0 \rightarrow S_2$ transition corresponds to a $\pi \rightarrow \pi^*$ excitation, with a significant charge transfer character, where electron density is displaced from the amino nitrogen to the nitro group, as can be seen in Figure 3. This makes the corresponding absorption band very sensitive to solvent polarity, and indeed, a strong solvatochromic shift is observed experimentally in polar solvents.[46,48,49]

In this work, we are mainly interested in the solvatochromic shift suffered by the $S_0 \rightarrow S_2$ band in solvent mixtures, in particular in mixtures of cyclohexane and triethylamine. In Table 4, we show the calculated values for the most intense absorption of PNA in the different solvent mixtures studied. We note that in solution the active transition is $S_0 \rightarrow S_1$; i.e., the charge transfer state that appears as S_2 in the gas phase is stabilized and becomes the lowest excited state, S_1, even in cyclohexane.

It is clear from Table 4 that absorption energies in solution are overestimated compared to the experimental values. The negligible solvatochromic shift obtained in pure CH (X_{TEA} = 0.00) with respect to the gas phase value is expected, since the ASEP/MD method includes only electrostatic interactions and solute polarization in the computation of transition energies, and these contributions are practically zero in CH. The experimental solvatochromic shift (3.87 vs 4.24 eV) is therefore

dx.doi.org/10.1021/jp310964k | J. Phys. Chem. B 2013, 117, 2466−2474

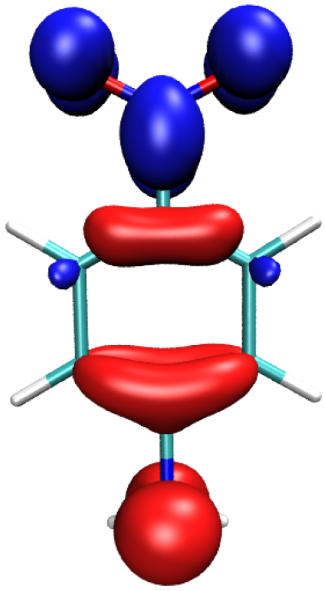

Figure 3. Electron density difference between the S_0 and S_2 states at the ground-state optimized geometry, in the gas phase. The electron density is higher in S_0 in the red regions and higher in S_2 in the blue regions. Isosurfaces drawn at a value of 0.003 e/a_o^3.

Table 4. Absorption Energy, in eV, to the S_1 State (Most Intense) of PNA in Mixtures of CH and TEA of Different Compositions

X_{TEA}	ΔE	exp.[46]
(CH) 0.00	4.32	3.87
0.09	4.16	
0.21	4.13	
0.42	4.08	
0.60	4.05	
0.79	4.04	
(TEA) 1.00	4.03	3.56

attributed to other interactions present in the system but considered constant in our method, such as dispersion, solvent electronic polarization, or solute−solvent electron exchange. The overestimation in the absorption energy is the same in TEA, meaning that the difference between CH and TEA, 0.3 eV, is very well reproduced by the theoretical calculations. This indicates that the error in the TEA calculation can be assigned to the same reasons mentioned above. In particular, the effect of dispersion and solvent polarization can be related to the refractive index of the solvent, and this quantity is very similar for both CH (1.43) and TEA (1.40); therefore, the error in both solvents is comparable.

Consequently, it is appropriate to analyze the shift of all the different solutions with respect to pure cyclohexane. In Figure 4, this solvent shift is represented for all the calculated mixtures along with the experimental values. In the figure, we have also represented the curve predicted by the dielectric enrichment model from ref 24; this model considers the effect of the change of solute dipole moment upon excitation in the mixture of solvents. The observed nonlinear behavior is correctly reproduced by the ASEP/MD calculations, while the dielectric enrichment model predicts too weak a nonlinearity. The latter fact is expected, given that the difference in dielectric constant between the two solvents is quite small (2.02 for CH, 2.42 for TEA).

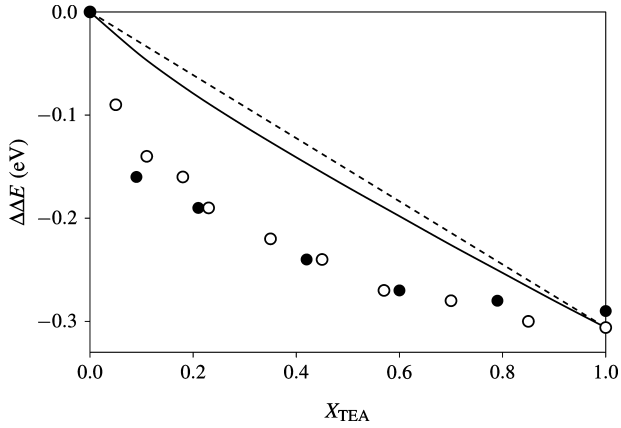

Figure 4. Relative shift, with respect to pure cyclohexane, of the main absorption band of PNA in mixtures of CH and TEA of varying composition (X_{TEA}). Black circles: ASEP/MD calculated values (this work). White circles: experimental values (ref 24). Continuous curve: dielectric enrichment behavior (ref 24).

The total solvatochromic shift can be partitioned, according to eq 2, into geometrical change, electronic distortion, and solute−solvent interaction. The resulting values in pure TEA solution are $\delta_{geo} = -0.06$, $\delta_{dist} = 0.05$, and $\delta_{int} = -0.28$, for a total shift of $\delta = -0.30$. Most of the shift is due to the difference in solute−solvent interaction between the ground and excited states (δ_{int}), while the geometrical and electronic components are much smaller, and practically cancel each other. Therefore, the rest of the discussion will be centered on the solute−solvent interaction, as the changes in the solute geometry and electron distribution have only a very limited effect on the absorption energies.

Other authors have suggested that the use of a purely electrostatic embedding in the quantum mechanical calculations, as used in this work, can create numerical instabilities, that manifest in a high dependence of the solvatochromic shift result on the basis set employed (see ref 18 and references therein). To check this possibility, we have performed test calculations with two additional basis sets. For this test calculation, the cc-pVDZ basis set, used in the rest of this work, yields a shift of −0.25 eV (this value does not include the δ_{geo} component). Under the same conditions, the results with 6-31G** and cc-pVTZ basis sets are, respectively, −0.25 and −0.23 eV. This shows that our results are quite stable to a change of basis set.

To determine the reasons behind the nonlinear trend in the solvatochromic shift, we first analyzed the composition of the solvation shell around the solute. In the system configurations extracted from the molecular dynamics simulations, we counted the number of molecules of each solvent species located at less than a given distance of the solute. We define this "distance" as the distance between any solute atom and the center of mass of the solvent molecule. The resulting local composition of the solvent, for a varying distance, is shown in Figure 5. For all the studied mixtures, the local TEA concentration near the solute molecule (Y_{TEA}) is significantly larger than the bulk concentration (X_{TEA}), up to a distance of around 5 Å. This proves that there is actually preferential solvation in this system.

Maitra and Bagchi[25,50] propose a formula that permits one to calculate the local molar fraction Y_{TEA} from the experimental values of the transition energies:

dx.doi.org/10.1021/jp310964k | J. Phys. Chem. B 2013, 117, 2466−2474

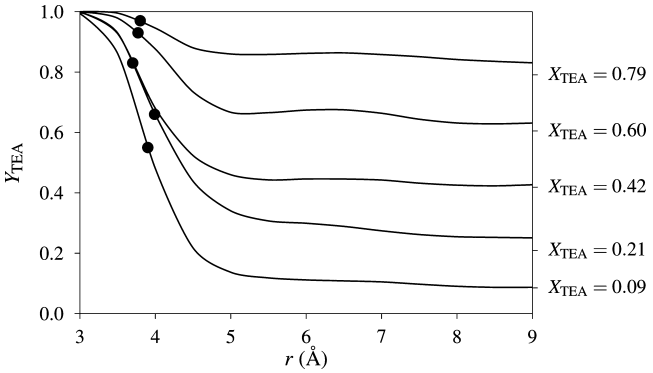

Figure 5. Local composition of the solvent (Y_{TEA}) around the PNA molecule as a function of the distance r (see text). Each curve corresponds to a different bulk solvent composition (X_{TEA}), which is indicated on the right edge. The values of Y_{TEA} obtained with eq 3 are indicated with circles.

$$Y_{TEA} = \frac{\Delta E(X_{TEA}) - \Delta E(0.00)}{\Delta E(1.00) - \Delta E(0.00)} \quad (3)$$

where $\Delta E(x)$ is the transition energy obtained for a bulk molar fraction x. The values provided by this equation are represented as black circles in Figure 5. All of them correspond to molar fractions found at distances between 3.7 and 4.0 Å around the solute molecule, which can be considered as the size of the first solvation shell.

As seen before, the nonspecific interactions responsible for the dielectric enrichment are not enough to account for the observed solvatochromic shifts. We therefore look for more specific interactions, and hydrogen bonds are the most conspicuous ones in this system, where they can be formed between the NH_2 group of PNA and the N of TEA. In Figure 6,

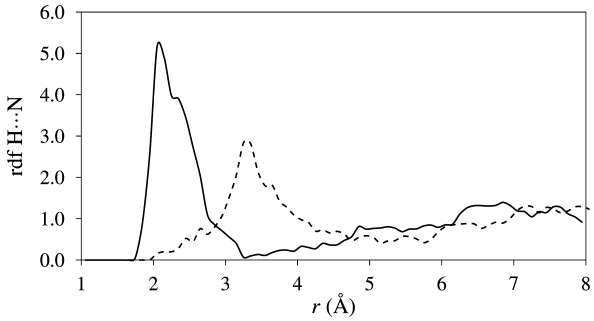

Figure 6. Radial distribution function of TEA N atoms around the amino group hydrogens of PNA, in pure TEA as solvent. Continuous and dashed lines correspond to the two chemically equivalent hydrogens.

we show the radial distribution functions of TEA nitrogen atoms around the two NH_2 hydrogens of PNA in pure TEA. Although the two hydrogens are chemically equivalent, the environment around a single molecule is not symmetric and therefore the two hydrogens show quite different radial distribution functions. One of the hydrogens has a maximum at around 2.0 Å and the other at 3.2 Å. When the configurations are examined, it is seen that both peaks are due to a single TEA molecule, which is located at the corresponding distance from the two solute hydrogens. The reason for this asymmetry can be found in two facts. First, the TEA molecules are bulky and steric hindrance prevents two TEA molecules from forming a hydrogen bond with each hydrogen atom. Second, the hydrogen bond formed is strong enough to be conserved during most of the simulation time, so that there's almost no displacement of TEA from one hydrogen to the other. Another consequence of the asymmetric environment can be found in Table 2, where the two N_9–H bonds have different lengths in TEA solution.

The asymmetric environment around the solute is found even when the simulations are performed with a perfectly symmetric solute geometry and charge distribution. This shows that the asymmetry introduced by a TEA molecule bonding to one of the amino nitrogens is relatively long-lived.

When we represent the average of the rdf's obtained for both amino hydrogens, and accounting for the relative concentration of TEA, we obtain very similar curves for all the studied values of X_{TEA}. As an example, in Figure 7, we show some of these

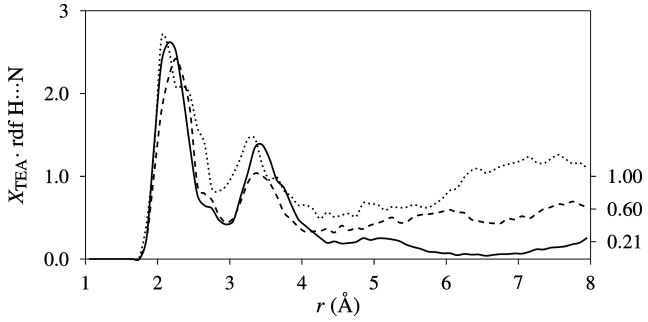

Figure 7. Average radial distribution function of the two amino group hydrogens of PNA, in solutions with X_{TEA} = 0.21 (solid line), X_{TEA} = 0.60 (dashed line), and X_{TEA} = 1.00 (dotted line). The rdf has been scaled by X_{TEA} to facilitate comparison between different solvent compositions. As a consequence, the long-distance value of each line is X_{TEA} and not 1 as usual in rdf's.

rdf's; it can be seen that the two peaks below 4 Å are very similar in all cases. In all solvent mixtures, the first peak is due to a single TEA molecule hydrogen-bonded to the solute, as given in Table 5. Careful examination of the configurations

Table 5. Coordination Numbers Calculated by Integrating the First Peak, up to ~2.9 Å, of the Average H···N rdf

X_{TEA}	n
0.09	0.98
0.21	1.05
0.42	0.98
0.60	0.97
0.79	1.07
(TEA) 1.00	1.01

shows that the second peak is due to the same TEA molecule but with respect to the other hydrogen atom of the amino group. Therefore, the two peaks actually correspond to one TEA molecule located at different distances from the two hydrogen atoms. This is confirmed by integration of the N···N rdf (Figure 8), which gives also approximately 1 molecule for the first peak. It is interesting to note that this first peak extends approximately up to 4 Å, which agrees with the size of the first solvation shell defined from the local molar fractions (see Figure 5).

In summary, even at the lowest TEA concentrations, a strong hydrogen bond is formed between the PNA solute molecule

dx.doi.org/10.1021/jp310964k | J. Phys. Chem. B 2013, 117, 2466–2474

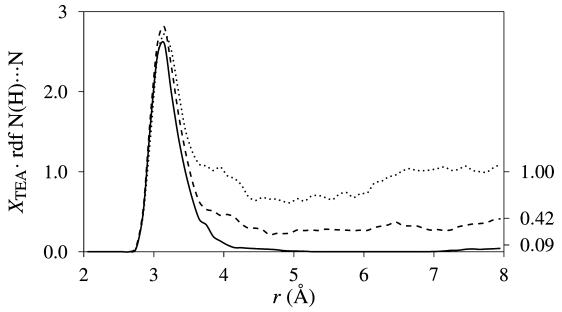

Figure 8. Radial distribution function of TEA N atoms around the amino nitrogen of PNA, in solutions with X_{TEA} = 0.09 (solid line), X_{TEA} = 0.42 (dashed line), and X_{TEA} = 1.00 (dotted line). The rdf has been scaled by X_{TEA} to facilitate comparison between different solvent compositions. As a consequence, the long-distance value of each line is X_{TEA} and not 1 as usual in rdf's.

and a TEA solvent molecule. This specific interaction accounts for most of the observed preferential solvation. To determine whether this hydrogen bond is also responsible for the important solvatochromic shift, we partition the solute−solvent interaction energy by solvent molecule.

After the normal ASEP/MD procedure has been carried out, the solute atomic charges are obtained for both the S_0 and S_1 states and their interaction with each solvent molecule in each configuration is computed classically. The difference between the interaction energies using the charges representing the excited and ground states gives the contribution of the interaction with each solvent molecule to the solvatochromic shift. The results, averaged over all configurations, are shown in Table 6, where it can be seen that the interaction with the first

Table 6. Contribution to the Electrostatic Component of the Solvatochromic Shift, in eV, of the Two TEA Molecules Closest to the NH_2 Group of the Solute, and All the Other Molecules, at the Different TEA Concentrations

X_{TEA}	first	second	third−*n*th
0.09	−0.13	0.00	−0.01
0.21	−0.11	−0.01	−0.03
0.42	−0.14	−0.03	−0.05
0.60	−0.13	−0.03	−0.08
0.79	−0.14	−0.05	−0.09
(TEA) 1.00	−0.14	−0.04	−0.11

TEA molecule, which forms a hydrogen bond with the NH_2 group, contributes around −0.13 eV to the solvatochromic shift. This value represents practically the total shift in the lowest TEA concentrations, and around half of the total shift in pure TEA. The fact that the contribution of the first molecule remains almost constant at all concentrations confirms that the structure of the hydrogen bond hardly changes, as was found when analyzing the rdf's.

To separate the effect of the first molecule, we calculate again the variation of the local solvent composition around the solute molecule but now ignoring the TEA molecule that forms a hydrogen bond with the PNA. The result is displayed in Figure 9. The conclusion is that for all solvent mixtures except X_{TEA} = 0.09 there is still a local increase of TEA concentration near the solute, and therefore that there is a preferential solvation effect that goes beyond the effect of the hydrogen bond.

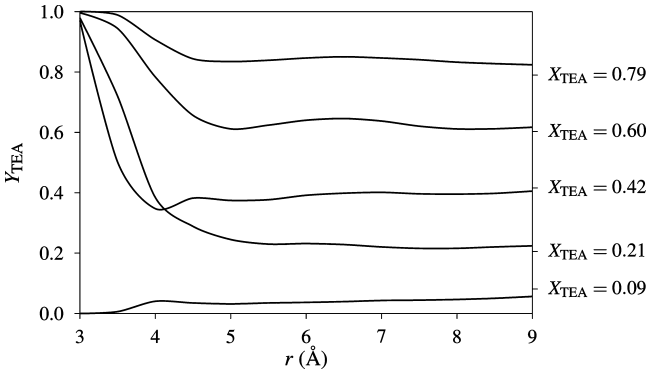

Figure 9. Same as Figure 5 but not counting the TEA molecule that forms the hydrogen bond with PNA.

In line with this, the contribution of the second molecule to the solvatochramic shift (Table 6) increases with the TEA concentration; this is due to the fact that the location of this second molecule is not as fixed as in the case of the first molecule, and it is found (on average) at shorter distances in the higher concentrations, which results in a larger contribution. The increase in the last column is due to the increasing number of TEA molecules in the simulation box. It is worth noting that these two effects show a nonlinear behavior too; there is a saturation effect when the TEA concentration increases.

To illustrate this, in Figure 10, we represent the three-dimensional average distribution of solvent molecules around the solute. It can be observed how at low TEA concentration a single TEA molecule is located near the NH_2 group. When the concentration increases, most TEA molecules are still located around the amino end, but the regions with an important CH density shrink, indicating that TEA molecules are partly occupying that volume. Already at X_{TEA} = 0.60, the CH molecules practically disappear from the first solvation shell.

Another analysis was carried out, but now partitioning the interaction energy component δ_{int} by chemical groups of the PNA molecule: the amino group, the nitro group, and the phenyl ring. With the same atomic charges for the two electronic states obtained above, we compute the interaction energy with the complete set of point charges representing the solvent in the ASEP/MD method. The interaction energy difference between the ground and excited states gives the total electrostatic contribution to the solvatochromic shift, and this can be partitioned by groups. It should be emphasized that the partition is only performed *a posteriori*, as an analysis tool, all calculations were done with the full QM/MM model. The result is shown in Figure 11. The phenyl group is practically inert and does not contribute significantly to the solvatochromic shift; its interaction with the solvent is almost unchanged between the ground state and the excited state. The nitro group has a slightly larger contribution, but the main effect comes from the interaction of the amino group. The negative sign indicates that the interaction of the amino group is stronger in the excited state than in the ground state, which is in agreement with the loss of electron density that occurs during the absorption (see Figure 3): the strength of the hydrogen bonds with TEA molecules is enhanced.

The interaction energy partitions, therefore, confirm that the formation of hydrogen bonds with TEA solvent molecules is the most important contribution to the solvatochromic shift. The observed nonlinear behavior can be attributed to a

dx.doi.org/10.1021/jp310964k | J. Phys. Chem. B 2013, 117, 2466−2474

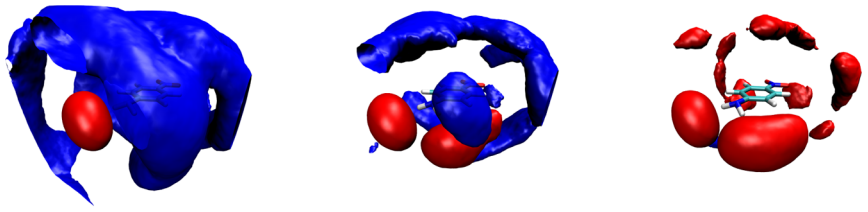

Figure 10. Distribution of the centers of mass of CH (in blue) and TEA (in red) molecules around the PNA molecule at three different X_{TEA} values. Isosurfaces shown for an occupancy value of 0.1, as calculated by VMD.[51]

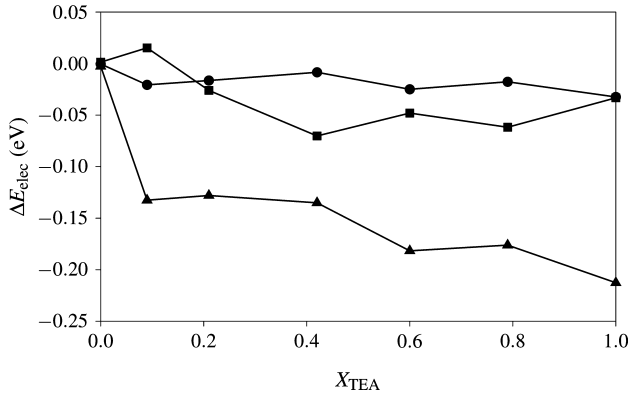

Figure 11. Contribution of the three chemical groups of PNA to the electrostatic component of the solvatochromic shift (difference in solute−solvent interaction energy between excited and ground state). Circles: phenyl ring. Squares: nitro group. Triangles: amino group.

combination of two factors: the strong hydrogen bond that forms even at very low TEA concentrations and some additional preferential solvation of TEA around the solute, the importance of this second factor being relatively minor.

CONCLUSIONS

The solvatochromic shift of the first absorption band of *para*-nitroaniline in mixtures of cyclohexane and triethylamine has been studied with a QM/MM method that applies the mean field approximation. The absorption energy changes nonlinearly with the solvent composition, closely matching the experimental behavior.

The electrostatic interaction between the amino group of the solute and the solvent accounts for the most part of the solvatochromic shift between cyclohexane and triethylamine. This is rationalized by the formation of a hydrogen bond where PNA acts as a proton donor and TEA as an acceptor, and this hydrogen bond is stronger in the excited state than in the ground state, which causes the bathochromic shift.

The hydrogen bond formed between the TEA and PNA molecules is long-lived and, given the size of the TEA molecule, which hinders the formation of a second hydrogen bond, determines an asymmetric environment around the solute PNA molecule.

In CH/TEA mixtures, it is found that the PNA−TEA hydrogen bond is formed even at the lowest TEA concentrations, which gives rise to the observed nonlinear behavior, as a small quantity of TEA added to the mixture can induce a relatively large solvatochromic shift.

It is therefore demonstrated that the nonlinearity in this system is mainly caused by preferential solvation due to the existence of specific interactions (hydrogen bonds), and not to the more general dielectric enrichment, in agreement with what had been suggested by previous studies.[24] While other authors could only proceed by elimination of dielectric enrichment to explain the experiments, in this work, the molecular reasons behind the experimental results have been directly observed.

AUTHOR INFORMATION

Corresponding Author

*E-mail: jellby@unex.es.

Notes

The authors declare no competing financial interest.

ACKNOWLEDGMENTS

This work was supported by the CTQ2011-25692 Project from the Ministerio de Economía y Competitividad of Spain, cofinanced by the European Regional Development Fund (ERDF), and the PRI08A056 Project from the Consejería de Empleo, Empresa e Innovación of the Gobierno de Extremadura. I.F.G. acknowledges the Gobierno de Extremadura and the European Social Fund for financial support.

REFERENCES

(1) Suppan, P. *J. Photochem. Photobiol., A* **1990**, *50*, 293−330.
(2) Reichardt, C. *Solvents and Solvent Effects in Organic Chemistry*, 3rd ed.; Wiley-VCH: Weinheim, Germany, 2003.
(3) Suppan, P. *J. Chem. Soc., Faraday Trans. 1* **1987**, *83*, 495−509.
(4) Silva, P. L.; Bastos, E. L.; El Seoud, O. A. *J. Phys. Chem. B* **2007**, *111*, 6173−6180.
(5) Navarro, A. M.; Garca, B.; Hoyuelos, F. J.; Peñacoba, I. A.; Leal, J. M. *J. Phys. Chem. B* **2011**, *115*, 10259−10269.
(6) Hisaindee, S.; Graham, J.; Rauf, M. A.; Nawaz, M. *J. Mol. Liq.* **2012**, *169*, 48−53.
(7) Saielli, G.; Bagno, A. *Phys. Chem. Chem. Phys.* **2010**, *12*, 2981−2988.
(8) Miertuš, S.; Scrocco, E.; Tomasi, J. *Chem. Phys.* **1981**, *55*, 117−129.
(9) Klamt, A.; Schüürmann, G. *J. Chem. Soc., Perkin Trans. 2* **1993**, *1993*, 799−805.
(10) Rivail, J.-L.; Rinaldi, D. *Chem. Phys.* **1976**, *18*, 233−242.
(11) Tomasi, J.; Mennucci, B.; Cammi, R. *Chem. Rev.* **2005**, *105*, 2999−3094.
(12) Basilevsky, M. V.; Odinokov, A. V.; Nikitina, E. A.; Petrov, N. C. *J. Electroanal. Chem.* **2011**, *660*, 339−346.
(13) Yamamoto, T. *J. Chem. Phys.* **2008**, *129*, 244104.
(14) Nakano, H.; Yamamoto, T. *J. Chem. Phys.* **2012**, *136*, 134107.
(15) Ten-no, S.; Hirata, F.; Kato, S. *J. Chem. Phys.* **1994**, *100*, 7443−4753.
(16) Sato, H.; Hirata, F.; Kato, S. *J. Chem. Phys.* **1996**, *105*, 1546−1551.
(17) Kaminski, J. W.; Gusarov, S.; Wesołowski, T. A.; Kovalenko, A. *J. Phys. Chem. A* **2010**, *114*, 6082−6096.
(18) Zhou, X.; Kaminski, J. W.; Wesołowski, T. A. *Phys. Chem. Chem. Phys.* **2011**, *13*, 10565−10576.

(19) Coutinho, K.; Canuto, S.; Zerner, M. C. *J. Chem. Phys.* **2000**, *112*, 9874−9880.
(20) Coutinho, K.; Georg, H. C.; Fonseca, T. L.; Ludwiga, V.; Canuto, S. *Chem. Phys. Lett.* **2007**, *437*, 148−152.
(21) Sánchez, M. L.; Aguilar, M. A.; Olivares del Valle, F. J. *J. Comput. Chem.* **1997**, *18*, 313−322.
(22) Fdez. Galván, I.; Sánchez, M. L.; Martín, M. E.; Olivares del Valle, F. J.; Aguilar, M. A. *Comput. Phys. Commun.* **2003**, *155*, 244−259.
(23) Aguilar, M. A.; Sánchez, M. L.; Martín, M. E.; Fdez. Galván, I. An Effective Hamiltonian Method from Simulations: ASEP/MD. In *Continuum Solvation Models in Chemical Physics*; Mennucci, B., Cammi, R., Eds., 1st ed.; Wiley: New York, 2007; Chapter 4.5, pp 580−592.
(24) Boggetti, H.; Anunziata, J. D.; Cattana, R.; Silber, J. J. *Spectrochim. Acta, Part A* **1994**, *50*, 719−726.
(25) Patel, S.; Gorai, S.; Malik, P. K. *J. Photochem. Photobiol., A* **2011**, *219*, 76−83.
(26) Fdez. Galván, I.; Sánchez, M. L.; Martín, M. E.; Olivares del Valle, F. J.; Aguilar, M. A. *J. Chem. Phys.* **2003**, *118*, 255−263.
(27) Okuyama-Yoshida, N.; Nagaoka, M.; Yamabe, T. *Int. J. Quantum Chem.* **1998**, *70*, 95−103.
(28) Roos, B. O.; Taylor, P. R.; Siegbahn, P. E. M. *Chem. Phys.* **1980**, *48*, 157−173.
(29) Andersson, K.; Malmqvist, P.-Å.; Roos, B. O.; Sadlej, A. J.; Wolinski, K. *J. Phys. Chem.* **1990**, *94*, 5483−5488.
(30) Andersson, K.; Malmqvist, P.-Å.; Roos, B. O. *J. Chem. Phys.* **1992**, *96*, 1218−1226.
(31) Ghigo, G.; Roos, B. O.; Malmqvist, P.-Å. *Chem. Phys. Lett.* **2004**, *396*, 142−149.
(32) Fdez. Galván, I.; Martín, M. E.; Muñoz-Losa, A.; Aguilar, M. A. *J. Chem. Theory Comput.* **2009**, *5*, 341−349.
(33) Valsson, O.; Filippi, C. *J. Chem. Theory Comput.* **2010**, *6*, 1275−1292.
(34) Fdez. Galván, I.; Martín, M. E.; Aguilar, M. A. *J. Chem. Theory Comput.* **2010**, *6*, 2445−2454.
(35) Fdez. Galván, I.; Martín, M. E.; Muñoz-Losa, A.; Sánchez, M. L.; Aguilar, M. A. *J. Chem. Theory Comput.* **2011**, *7*, 1850−1857.
(36) Fdez. Galván, I.; Martín, M. E.; Muñoz-Losa, A.; Aguilar, M. A. *J. Chem. Theory Comput.* **2011**, *7*, 3694−3701.
(37) Jorgensen, W. L.; Maxwell, D. S.; Tirado-Rives, J. *J. Am. Chem. Soc.* **1996**, *118*, 11225−11236.
(38) Karlström, G.; Lindh, R.; Malmqvist, P.-Å.; Roos, B. O.; Ryde, U.; Veryazov, V.; Widmark, P.-O.; Cossi, M.; Schimmelpfennig, B.; Neogrády, P.; Seijo, L. *Comput. Mater. Sci.* **2003**, *28*, 222−239.
(39) Refson, K. *Comput. Phys. Commun.* **2000**, *126*, 310−329.
(40) Trueblood, K. N.; Goldish, E.; Donohue, J. *Acta Crystallogr.* **1961**, *14*, 1009−1017.
(41) Panunto, T. W.; Urbanczyk-Lipkowska, Z.; Johnson, R.; Etter, M. C. *J. Am. Chem. Soc.* **1987**, *109*, 7786−7797.
(42) Reis, H.; Grzybowski, A.; Papadopoulos, M. G. *J. Phys. Chem. A* **2005**, *109*, 10106−10120.
(43) Jones, M. E.; Taft, R. W.; Kamlet, M. J. *J. Am. Chem. Soc.* **1977**, *99*, 8452−8453.
(44) Moran, A. M.; Kelley, A. M.; Tretiak, S. *Chem. Phys. Lett.* **2003**, *367*, 293−307.
(45) Scalmani, G.; Frisch, M. J.; Mennucci, B.; Tomasi, J.; Cammi, R.; Barone, V. *J. Chem. Phys.* **2006**, *124*, 094107.
(46) Millefiori, S.; Favini, G.; Millefiori, A.; Grasso, D. *Spectrochim. Acta, Part A* **1977**, *33*, 21−27.
(47) Kosenkov, D.; Slipchenko, L. V. *J. Phys. Chem. A* **2011**, *115*, 392−401.
(48) Kovalenko, S. A.; Schanz, R.; Farztdinov, V. M.; Hennig, H.; Ernsting, N. P. *Chem. Phys. Lett.* **2000**, *323*, 312−322.
(49) Moran, A. M.; Kelley, A. M. *J. Chem. Phys.* **2001**, *115*, 912−924.
(50) Maitra, A.; Bagchi, S. *J. Phys. Chem. B* **2008**, *112*, 2056−2062.
(51) Humphrey, W.; Dalke, A.; Schulten, K. *J. Mol. Graphics* **1996**, *14*, 33−38.